Journal of Power Sources 390 (2018) 134–141

Contents lists available at ScienceDirect

Journal of Power Sources

journal homepage: www.elsevier.com/locate/jpowsour

Enhancing the performance of planar heterojunction perovskite solar cells using stable semiquinone and amine radical modified hole transport layer

Chunhua Wang[a], Yuan Li[b,***], Chujun Zhang[a], Liyang Shi[c], Sichao Tong[a], Bin Guo[b], Jian Zhang[d], Jun He[a], Yongli Gao[a,e], Chaohao Su[c,**], Junliang Yang[a,*]

[a] Institute of Super-microstructure and Ultrafast Process in Advanced Materials, School of Physics and Electronics, Central South University, Changsha, 410083, PR China
[b] Institute of Polymer Optoelectronic Materials and Devices, State Key Laboratory of Luminescent Materials and Devices, South China University of Technology, Guangzhou, 510640, PR China
[c] Architectural Design & Research Institute of South China University of Technology, Guangzhou, 510640, PR China
[d] School of Material Science and Engineering, Guilin University of Electronic Technology, Guilin, 541004, PR China
[e] Department of Physics and Astronomy, University of Rochester, Rochester, NY, 14627, USA

HIGHLIGHTS

- Dopamine radical enhanced the PCE and device durability.
- PEDOT with high work function was obtained via semiquinone containing backbone.
- The HTL with excellent hole transport and efficient electron blocking.
- The PCE over 15.3% was achieved for PSCs with a simple planar heterojunction structure.

ARTICLE INFO

Keywords:
Perovskite solar cells
Planar heterojunction
Hole transport layer
Work function

ABSTRACT

Highly efficient organic-inorganic hybrid planar heterojunction perovskite solar cells with an architecture of indium tin oxide (ITO)/PEDOT:PSS-NH_2-OH/$CH_3NH_3PbI_3$/PCBM/Al are fabricated *via* one-step, solution process by employing the dopamine modified PEDOT:PSS (PEDOT:PSS-NH_2-OH) as the hole transport layer, of which the power conversion efficiency of 15.34% is achieved with negligible hysteresis regardless of different scanning directions and scanning speeds. The average efficiency of twenty devices with PEDOT:PSS-NH_2-OH is increased to 14.16% from 10.67% with PEDOT:PSS, and the former devices exhibit good reproducibility with small standard deviations. Cyclic voltammetry results show that the highest occupied molecular orbital energy level of PEDOT:PSS-NH_2-OH (5.32 eV) matches well with the valence band of $CH_3NH_3PbI_3$ absorbers (5.4 eV). Photoluminescence measurements indicate that the $CH_3NH_3PbI_3$ film deposited on PEDOT:PSS-NH_2-OH has strong charge extraction capability than that on PEDOT:PSS. Electrochemical impedance spectroscopy results suggest that the photovoltaic devices exhibit efficient hole transport and excellent electron blocking employing PEDOT:PSS-NH_2-OH as the hole transport layer, as well as have low series, contact resistance and large recombination resistance. The research demonstrates that the stable semiquinone and amine radical modified PEDOT:PSS can acts as an outstanding hole transport material for fabricating high-efficient perovskite solar cells.

1. Introduction

Organic-inorganic hybrid perovskite solar cells (PSCs) as a hotspot in academia in recent years have captured enormous attention owing to the great superiorities of perovskite materials, such as ambipolar properties, direct band gap, strong absorption, high carrier mobility, long carrier diffusion, low exciton binding energy, *etc.* [1–4]. There has been an awe-inspiring breakthrough in photovoltaic community by multidisciplinary efforts, resulting in the state-of-the-art of power conversion efficiency (*PCE*) of PSC up to 22.7% [5]. Mesoscopic structural and planar-based PSCs have been widely studied in past years. Planar heterojunction (PHJ) PSCs, especially inverted PHJ-PSCs,

* Corresponding author.
** Corresponding author.
*** Corresponding author.
E-mail addresses: celiy@scut.edu.cn (Y. Li), suchaohao@scut.edu.cn (C. Su), junliang.yang@csu.edu.cn (J. Yang).

https://doi.org/10.1016/j.jpowsour.2018.04.049
Received 27 January 2018; Received in revised form 5 April 2018; Accepted 13 April 2018

have been attracting much attention due to the simple architecture and inconspicuous hysteresis, as well as the low-cost, low-temperature, solution processing and matching with high-output, large-scale roll-to-roll printing techniques [6–9].

It is well recognized that the active layer of photovoltaic devices absorb sunlight and produce electrons and holes separated, which then transport to electron transport layer (ETL) and hole transport layer (HTL), respectively, and ultimately are collected by the electrodes. Efficient carrier extraction and transport play the key role on device performance parameters such as open-circuit voltage (V_{oc}), *PCE* and hysteresis [10–14]. The poly(3,4-ethylenedioxythiophene)/poly(styrenesulfonicacid) (PEDOT:PSS) is one of the main HTL materials employed in solar cells [15,16]. But, due to its intrinsic properties of acidity and hygroscopicity, it is unfavorable to achieve long-term stability. As a good HTL, it not only needs high electrical conductivity and excellent optical transparency with wide bandgap, but also it should be an outstanding electron blocking property with preeminent hole transport. Many studies have been done for probing alternative HTL materials, for instance, metal oxides MoO_3 [15,16], WO_3 [17,18], V_2O_5 [19], CuI [20], NiO_x [21–23], PbS quantum dots [24], CuSCN films [25] and so on.

Motivated by our previous work on the stable semiquinone radical and efficient modification of ITO work function [10], we systematically investigated the effects of dopamine (DA) doping on electron donating capability of PEDOT:PSS and perovskite film quality as well as the charge recombination kinetics in the solar cells. In comparison with the pristine PEDOT:PSS, we found that DA doping endows PEDOT:PSS with higher radical content and stronger charge extraction capability from perovskite to HTLs [11]. PEDOT:PSS-NH_2-OH with typical semiconductor behavior exhibits more efficient electron donating effect than PEDOT:PSS due to the further doping of DA-PEDOT: PSS on perovskite layer during device fabrication, thereby providing better trap passivation capability. Besides improving perovskite film crystallinity, DA with amino and hydroxyl groups interacts with the undercoordinated Pb atoms on the perovskite crystal, resulting in the reduced surface recombination. Due to the electron transfer process of phenol-quinone-PEDOT backbone, PEDOT:PSS-NH_2-OH with deep work function (−5.32 eV) exhibits better capability to suppress the interfacial trap-assisted recombination with longer charge recombination lifetime and higher charge extraction rate. Eventually, the *Voc, FF* and *PCE* of the PEDOT:PSS-based devices simultaneously increased from 0.86 V, 69.3% and 12.01% to 0.97 V, 78.15% and 15.34% when PEDOT:PSS-NH_2-OH was introduced.

Our molecular design was presented in Scheme 1. The amino and hydroxyl radical dual-functionalization of DA endows PEDOT:PSS with several excellent properties: 1) High radical content and strong charge extraction capability from perovskite to HTL. 2) Desirable energy level alignment with perovskite. 3) Favorable interaction with perovskite for high-quality film formation. 4) Efficient surface trap passivation effects for perovskite film with a long charge recombination lifetime and high charge extraction rate. With these multiple functions, it was succeed to apply in perovskite $CH_3NH_3PbI_3$ ($MAPbI_3$) photovoltaic devices with a structure of ITO/PEDOT:PSS-NH_2-OH/$MAPbI_3$/PCBM/Al that fabricated by one-step, solution-processing under low temperature. As a result, encouraging results with sharply enhanced performance (a *PCE* of 15.34%) were achieved as compared to PEDOT:PSS-based PHJ-PSCs (a *PCE* of 12.01%) with negligible hysteresis regardless of scanning directions and scanning speeds. These in-depth understanding of structure-performance clearly provide new guideline to design effective HTLs inspired by the electron transfer of semiquinone radical, phenol derivatives for further improvements of inverted PHJ-PSCs.

2. Experiment section

2.1. Materials

Methylammonium iodide (CH_3NH_3I, MAI, 99%) and lead iodide (PbI_2, 99%) were purchased from Wuhan Jingge and Shanghai Zhengpin, respectively. N,N-Dimethylformamide (Super dry, DMF) and chlorobenzene (Super dry, CB) were provided by J&K Seal. Fullerene derivative [6,6]-phenyl-C61-butyric acid methyl ester (PCBM, Dye Source, American) was supplied by American Dye Source. PEDOT: PSS (PVP AI 4083) was purchased from Baytron.

2.2. Preparation of PEDOT:PSS-NH_2-OH

PEDOT:PSS-NH_2-OH was synthesized as following detailed process: 20 g polystyrene sulfonic acid (PSS, Mw = 75000 Da, 30 wt.%) and 1 g of 3,4-ethylenedioxy thiophene (EDOT) and was mixed, and the solution was adjusted to pH = 2. Then, PEDOT:PSS-NH_2-OH (1% in water, v/v) was prepared by adding the product above into the PEDOT:PSS-4083 solution with the ratio of 1:5 (v/v). Dopamine-copolymerized PEDOT:PSS was obtained and studied carefully. The molecular structure, UV-vis absorption properties of modified PEDOT:PSS were also investigated. The molecular structure of PEDOT:PSS-NH_2-OH is proposed and shown in Scheme 1. All the chemicals were used as received without further purification.

2.3. Precursor preparation

The perovskite precursor was prepared by dissolving MAI and PbI_2 at a molar ratio of 1:1 in anhydrous DMF at the concentration of 550 mg/ml. PCBM was dissolved in anhydrous CB with a concentration of 15 mg/ml. Perovskite precursor solution and PCBM solution were energetically stirred over night at 60 °C to ensure dissolve adequately. A 0.22 μm PVDF filter was employed to filter the perovskite precursor before deposition.

2.4. Device fabrication

The inverted PHJ-PSC with the structure of ITO/HTL/$MAPbI_3$/PCBM/Al were fabricated in this study. The patterned indium tin oxide (ITO) glass substrate was ultrasonically cleaned in acetone, detergents, distilled water and isopropyl alcohol for 20 min, respectively. After the cleaning and drying by nitrogen flow, the ITO-coated substrate was treated using UV-ozone for 20 min to reform and removal of organic substance. The HTL materials PEDOT:PSS and PEDOT:PSS-NH_2-OH were spin-coated on the ITO substrate at a spinning speed of 3000 rpm for 30 s and 4000 rpm for 30 s, and then annealed on hot plate at 150 °C for 15 min and 110 °C for 10 min, respectively, resulting in a thickness of about 35 nm for PEDOT:PSS and 30 nm for PEDOT:PSS-NH_2-OH. It is noted that the PEDOT:PSS solution was agitated for 20 min and PEDOT:PSS-NH_2-OH solution was ultrasonically for 10 min before spin-coating. The solvent-induced-fast-crystallization deposition method [14,27–29] was used to fabricate the perovskite layer to obtain dense and smooth high-quality perovskite film in a nitrogen-filled glovebox (both H_2O and O_2 < 1.0 ppm), and *ca.* 300 nm thick of red brown $MAPbI_3$ perovskite film can be obtained ultimately. PCBM solution was spin-coated onto perovskite layer at a speed of 3000 rpm for 30 s, resulting in a thickness about 30 nm. Finally, a 100 nm Al electrode was deposited by thermal evaporation under a vacuum of about 8.0×10^{-6} mbar, the active area of the devices is 0.09 cm^2 that determined by the size of Al pads.

2.5. Characterization

The absorption spectra, crystallographic properties, morphologies of perovskite films were characterized by employing ultraviolet-visible

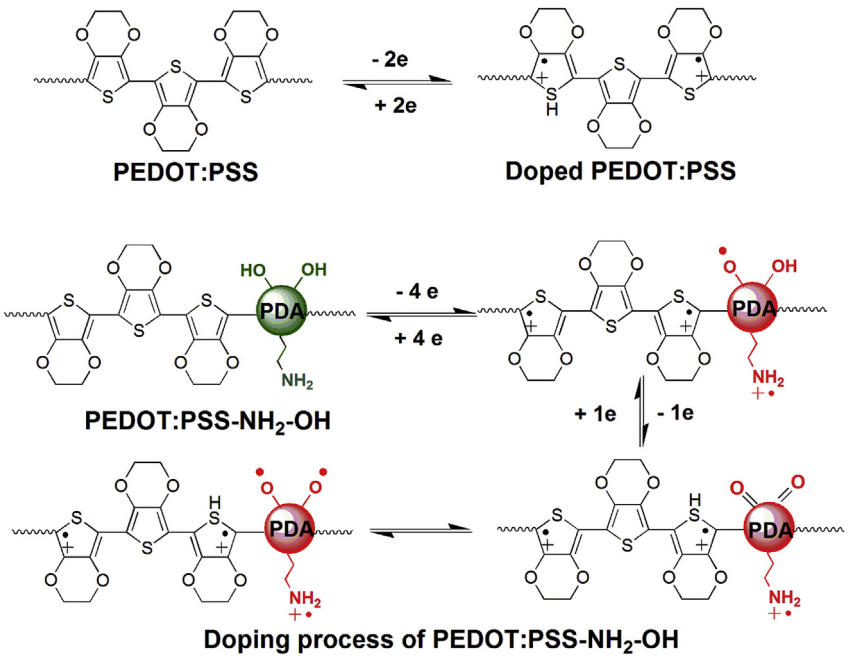

Scheme 1. The very different doping process of PEDOT:PSS and PEDOT:PSS-NH_2-OH in which dopamine semiquinone radical provides more electron donating effect for the trap passivation (see the blue-shift of PL in Fig. 6c).

spectrophotometer (UV-vis, Puxi, T9, China), X-ray diffractometer (XRD, Rigaku D, Max 2500, Japan) and scanning electron microscope (SEM, FEI Helios Nanolab 600i, America), respectively. Thin film thickness of PHJ-PSCs and the surface roughness of perovskite films were obtained by surface profilometer (Dektak 150, Veeco, USA) and atomic force microscope (AFM, Agilent Technologies 5500AFM/SPM System). Steady-state PL and time-resolved PL spectra were achieved using intensified charge coupled device detector (ICCD, DH334T-18U-03) and time-correlated single photon counting (TCSPC, MS3504I) measurements. Cyclic voltammetry (CV, CHI606D, Chenhua, Shanghai) test was conducted with a film on glassy carbon electrode against Ag/AgCl (3 M KCl solution) reference electrode at scanning rate 100 mV/s. Current density-voltage (*J-V*) characteristics of PHJ-PSCs devices were measured by digital Source Meter (Keithley, model 2420, USA) that standard silicon simulator was employed to calibrate the light intensity with the standard value 100 mW/cm^2. The *PCEs* were measured using a solar simulator (Newport 91160s, AM 1.5G, USA) at 300 mV/s from −1.5 V to +1.5 V if without otherwise specified. The characteristics of carrier transport and recombination were evaluated by electrochemical impedance spectroscopy (EIS, CHI606D, Chenhua, Shanghai). Incident photon to current conversion efficiency (IPCE, Saifan, Beijing) spectra of PHJ-PSC devices were performed and analyzed by quantum efficiency measurement system.

3. Results and discussion

UV-vis was used to characterize the property of PEDOT:PSS-NH_2-OH. UV-vis spectra of PEDOT:PSS and PEDOT:PSS-NH_2-OH aqueous dispersions are shown in Fig. 1a. It is clear that PEDOT:PSS-NH_2-OH has stronger absorption intensity than the pristine PEDOT:PSS, and it also has a visible region between 200 and 300 nm, owning to the introduction of dopamine. Thus, more light would be absorbed when employ PEDOT:PSS-NH_2-OH and this will enhance the device durability considering the UV-sensitivity of perovskite solar cells. Besides, PEDOT:PSS-NH_2-OH in aqueous dispersion exhibited the broad absorption from 550 to 1000 nm. The result demonstrated that PEDOT:PSS-NH_2-OH had been successfully prepared. Furthermore, the transmittance spectra of PEDOT:PSS-NH_2-OH and PEDOT:PSS films were investigated in this work as shown in Fig. 1b. The broad peak from 550 to 900 nm increased a lot as compared with the original PEDOT:PSS, which is in accordance with the UV-vis absorption results. Besides, time-dependence contact angle of PEDOT:PSS and PEDOT:PSS-NH_2-OH films were also studied (Fig. S1), there was a slight drop for PEDOT:PSS-NH_2-OH (decreased from 53° to 42° with the exposure time increased from 1 min to 3 min) while almost no change happened on PEDOT:PSS film compared with PEDOT:PSS under the same condition. In contrast, our PEDOT:PSS-NH_2-OH showed much better hydrophobicity which will enhance the device stability [4].

Herein, PHJ-PSCs photovoltaic devices with a simple architecture of ITO/HTL/$MAPbI_3$/PCBM/Al were fabricated *via* one-step, solution process by employing the PEDOT:PSS-NH_2-OH as the hole transport layer to examine the PEDOT:PSS-NH_2-OH properties. It is perceived that the quality of perovskite thin film plays the key role in determining the performance of photovoltaic devices. Here, solvent-induced-fast-crystallization deposition method was employed to gain dense and uniform films [14,27–29]. The surface morphology of $MAPbI_3$ thin film deposited onto PEDOT:PSS or PEDOT:PSS-NH_2-OH characterized by SEM is presented in Fig. 2a–b, showing that the thin films are compact and flat without pin-holes. It suggests that high-quality perovskite film can be achieved as spin-coating onto ITO/PEDOT:PSS-NH_2-OH substrates. Furthermore, the result shows that the grains size of perovskite film on PEDOT:PSS-NH_2-OH is larger than that on conventional PEDOT:PSS. The inset in Fig. 1b demonstrates the grain size distribution of $MAPbI_3$ thin film on PEDOT:PSS-NH_2-OH and PEDOT:PSS, of which the average grain size are about 271 nm and 230 nm, respectively. The cross-sectional SEM image of $MAPbI_3$ film on PEDOT:PSS-NH_2-OH is shown in Fig. 2c, the vertical scan picture presents that dense and uniform grain well-distribute in the interior of $MAPbI_3$ perovskite system, and the film thickness is about 300 nm.

Fig. 2d exhibits the XRD patterns of perovskite films deposited on PEDOT:PSS and PEDOT:PSS-NH_2-OH substrates, where the characteristic peaks of perovskite are observed clearly. The intensities and widths of diffraction peaks exhibited at 14.2°, 28.56°, 32.00°, 40.77° and 43.31° are similar for $MAPbI_3$ perovskite films on both PEDOT:PSS and PEDOT:PSS-NH_2-OH substrates, which can be assigned to (110), (220), (310), (224) and (314) crystal faces, respectively [30]. Generally, the preferential growth of $MAPbI_3$ films at (110) lattice plane is attributed to the tetragonal structure, resulting in strong diffraction peaks of (110)

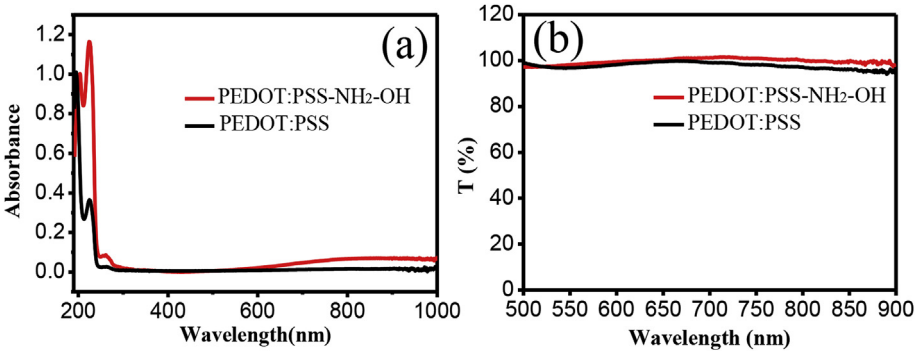

Fig. 1. (a) UV-vis spectra and (b) transmittance spectra of PEDOT:PSS and PEDOT:PSS-NH_2-OH.

and (220) [31]. The sharp diffraction peaks again certified $MAPbI_3$ thin films are highly crystallized.

CV test was employed to study the redox process of our product, as shown in Fig. 3a, it is interesting to find that the work function (WF) level of PEDOT:PSS-NH_2-OH presented an impressive increased and was much higher than 5.0 eV of the original PEDOT:PSS. The WF changed from 5.0 eV to 5.32 eV. The decrease of HOMO actually means that the work function (WF) is enhanced accordingly. The WF of the interface layer would significantly affect the *Voc* of the PSCs because the *Voc* is associated with energy loss [26,27]. Considering the energy level matches well with the valence band of $MAPbI_3$ absorbers (Fig. 3b) that is beneficial for hole transport, resulting from a reduction in the energy loss during the hole migration from the valence band of $MAPbI_3$ to HTL, and thus potentially lead to a larger *Voc* [27].

Abnormal hysteresis of *J-V* characteristic curves in PSCs has been widely reported and is considered as a serious obstacle for photovoltaic performance. Herein, typical *J-V* curves of PHJ-PSC photovoltaic devices with PEDOT:PSS and PEDOT:PSS-NH_2-OH HTL are exhibited in Fig. 4a and b accordingly, which is deduce from the typical PHJ-PSC devices. It shows that the *PCE* of 15.34% could be achieved for PHJ-PSCs employing the PEDOT:PSS-NH_2-OH as the HTL under forward scanning direction from −1.5 V to +1.5 V, of which the V_{oc}, J_{sc} and *FF* are 0.97 V, 20.22 mA/cm^2, 78.15%, respectively. Under the reverse scanning direction, the *PCE* of 14.60% with V_{oc} 0.97 V, J_{sc} of 19.97 mA/cm^2 and *FF* of 75.36% could be achieved as well. They present an

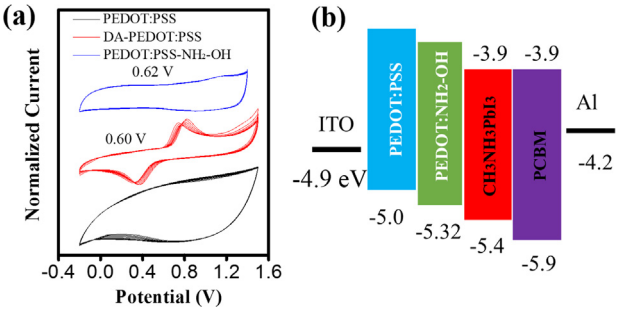

Fig. 3. (a) CV curves of PEDOT:PSS and PEDOT:PSS-NH_2-OH film in anhydrous dichloromethane using 0.1 M Bu_4NPF_6 as electrolyte and it was scanned for 10 runs at a scan rate of 100 mV s^{-1}. The HOMO level was calculated according to HOMO = − (E_{OX}+4.7) eV. (b) The energy band diagram of PHJ-PSCs.

impressive enhancement than the reference PHJ-PSCs with PEDOT:PSS as the HTL (12.01%). In addition, the measurement with different scanning speeds of 500 mV/s, 300 mV/s, 150 mV/s, and 100 mV/s were carried out, as shown in Fig. 4c, of which the *PCEs* are 14.89%, 15.34%, 14.64% and 14.32%, correspondingly. The results indicate that there is scarcely distinct hysteresis regardless of the scanning direction and scanning speed.

Fig. 4d presents the statistical distribution of the *PCEs* based on

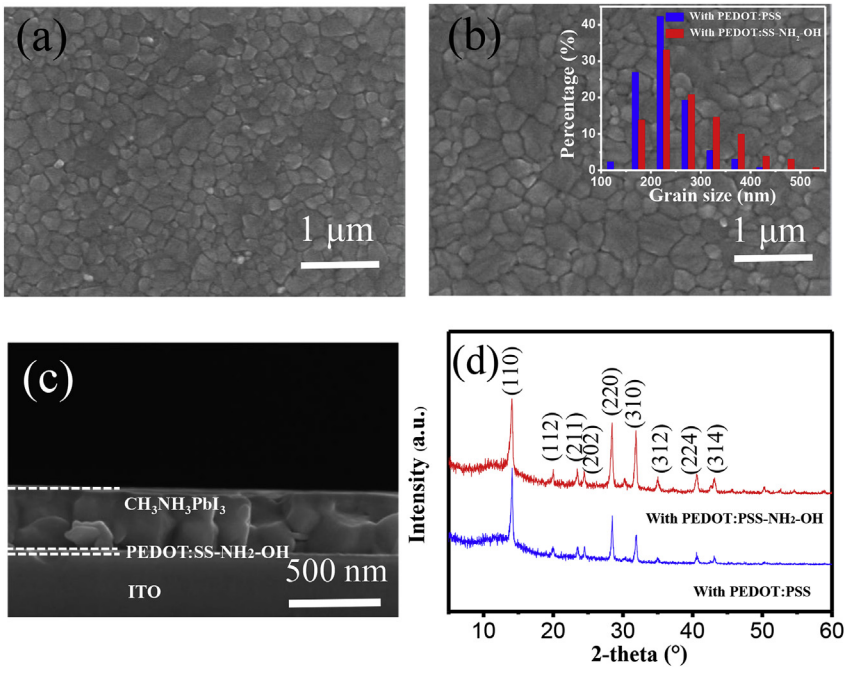

Fig. 2. (a–b) SEM morphology images of $MAPbI_3$ film deposited onto PEDOT:PSS and PEDOT:PSS-NH_2-OH, respectively. The insert in b presents the distribution of grain size for two type perovskite films. (c) Cross-sectional SEM image of $MAPbI_3$ film on PEDOT:PSS-NH_2-OH. (d) XRD patterns of $MAPbI_3$ films on PEDOT:PSS and PEDOT:PSS-NH_2-OH HTL, respectively.

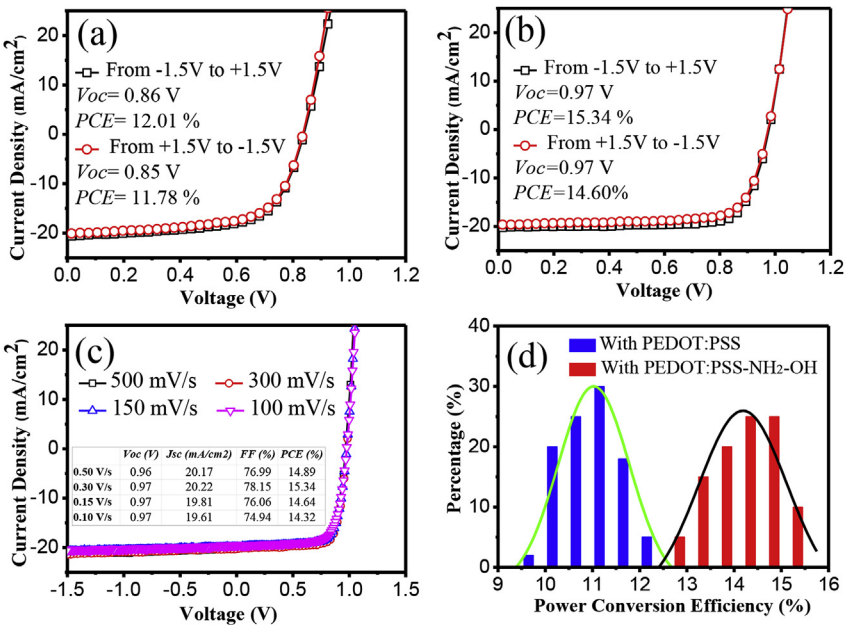

Fig. 4. (a–b) The typical *J-V* curves of PHJ-PSCs with PEDOT:PSS and PEDOT:PSS-NH_2-OH HTL materials that measured with forward and reverse scanning directions. (c) *J-V* characteristic curves of PEDOT:PSS-NH_2-OH -based device with different scanning speeds under AM 1.5 G illumination. (d) The distribution of the *PCEs* obtained from 20 PHJ-PSC photovoltaic devices with the PEDOT: PSS or PEDOT:PSS-NH_2-OH HTL.

twenty PHJ-PSC photovoltaic devices with pristine PEDOT:PSS and synthetic PEDOT:PSS-NH_2-OH films as the HTL, respectively, in which the devices were fabricated under the same condition except for the HTL material. According to the distribution of number of devices, the trend of *PCEs* was obtained by Gauss function fitting, as shown in graph with curves drawing. It is obvious that the *PCE* of PEDOT:PSS-NH_2-OH-based devices show a clear advantage than pristine devices with significantly improvement, and the best *PCE* of device is over 15%, resulting in the average *PCE* enhanced markedly from 10.67% to 14.16% with an enhancement of 32.7%. Besides, it also found that all the devices fabricated with PEDOT:PSS-NH_2-OH show small fluctuations for performance parameters, which shows good repeatability and operability.

To objectively uncover the superiorities of photovoltaic devices with PEDOT:PSS-NH_2-OH as the HTL, the same batch PHJ-PSCs with PEDOT:PSS and PEDOT:PSS-NH_2-OH HTL were manufactured, and the statistical results were analyzed. Fig. 5a–d exhibits the distribution of the performance parameters, *i.e.*, V_{oc}, J_{sc}, *FF* and *PCE* that based on twenty PHJ-PSC devices with PEDOT:PSS and PEDOT:PSS-NH_2-OH, respectively. It turned out that as the PEDOT:PSS is substituted by PEDOT:PSS-NH_2-OH, all photovoltaic parameters have improved greatly, of which the average performance parameters of V_{oc}, J_{sc}, *FF* and *PCE* are 0.96 V, 19.73 mA/cm^2, 74.77% and 14.16%, respectively, which are much higher than the average parameters of PHJ-PSCs with PEDOT:PSS (V_{oc}, J_{sc}, *FF* and *PCE* are 0.86 V, 18.22 mA/cm^2, 68.62% and 10.67%, respectively), resulting in the enhancement of about 11%, 8%, 9% and 33%, respectively. Here, the marked improvement of V_{oc} for PEDOT:PSS-NH_2-OH-based photovoltaic devices can be linked to the larger grains size owing to it can reduce interfacial area, as a result, suppress charge trapping and decrease bulk defects as well as the well

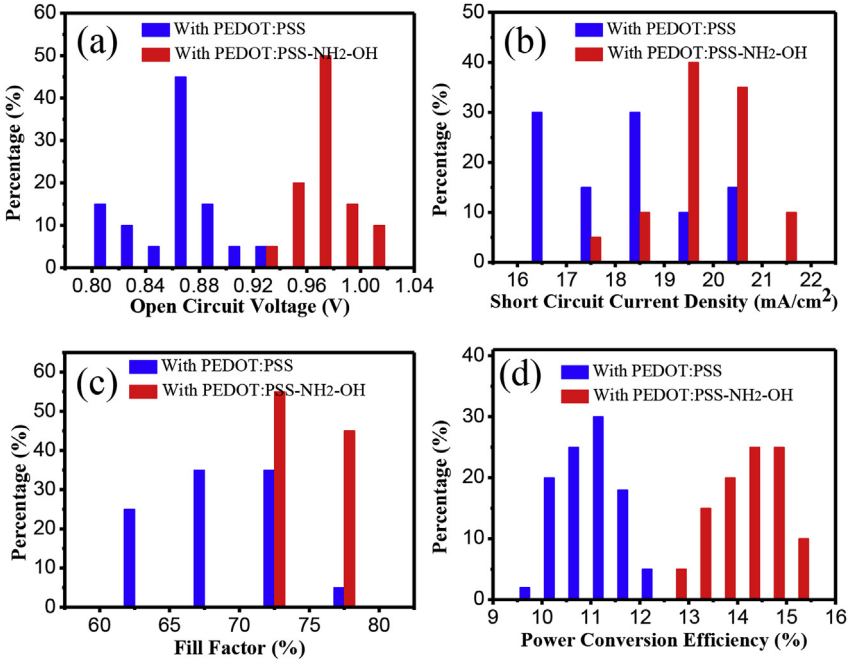

Fig. 5. The statistic performance parameters (a) V_{oc}, (b) J_{sc}, (c) *FF* and (d) *PCE* for PHJ-PSC devices with PEDOT:PSS and PEDOT:PSS-NH_2-OH, respectively.

Table 1
The performance parameters obtained from *J-V* curves for PHJ-PSC devices with PEDOT: PSS and PEDOT:PSS-NH_2-OH HTL. The best photovoltaic parameters are shown in the bracket.

Samples	*Voc* (*V*)	*Jsc* (mA/cm^2)	*FF* (%)	*PCE* (%)
With PEDOT:PSS	0.86 ± 0.031 (0.92)	18.22 ± 1.454 (21.02)	68.62 ± 4.398 (76.1)	10.67 ± 0.608 (12.01)
With PEDOT:PSS-NH_2-OH	0.96 ± 0.025 (1.00)	19.73 ± 0.904 (21.06)	74.77 ± 1.703 (78.15)	14.16 ± 0.642 (15.34)

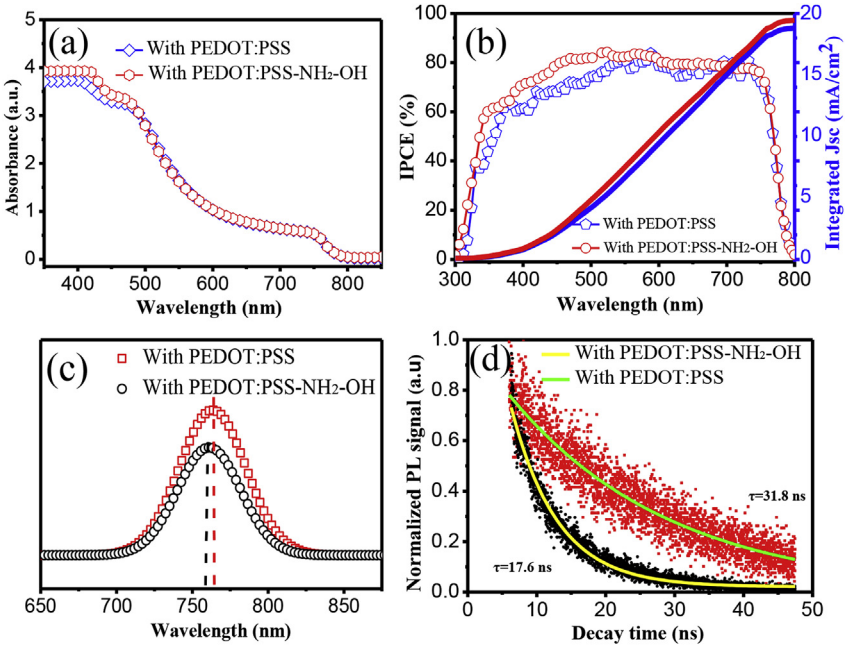

Fig. 6. (a) Absorption spectra of $MAPbI_3$ films deposited onto PEDOT:PSS or PEDOT:PSS-NH_2-OH. (b) IPCE spectrum for PHJ-PSCs devices with PEDOT:PSS or PEDOT:PSS-NH_2-OH HTL material, respectively, and integrated *Jsc* are also presented correspondingly. (c–d) Steady photoluminescence (PL) and time-resolved PL spectra of $MAPbI_3$ thin films based on PEDOT:PSS or PEDOT:PSS-NH_2-OH THL.

band match of PEDOT:PSS-NH_2-OH and $MAPbI_3$ [10,11,32]. Moreover, it is worth noting that all the parameters distribution more evenly with small standard deviations (Table 1), indicating the excellent repeatability and reliability. The sharp improvement of photovoltaic perovskite could be attributed to the interface improvement between HTL and perovskite film, and the detail reasons can be analyze by EIS analysis (see the subsequent EIS study). The detail parameters are listed in Table 1.

Absorption spectra of $MAPbI_3$ films deposited on PEDOT:PSS-NH_2-OH or PEDOT:PSS substrates are also measured as shown in Fig. 6a. It exhibits that the $MAPbI_3$ thin film shows strong absorption, which is similar to $MAPbI_3$ perovskite thin film on PEDOT:PSS, suggesting the strong photon harvesting capability for the spectral range from 350 nm to 850 nm. However, it is worthwhile note that the higher absorption on short wave (350–500 nm) for PEDOT:PSS-NH_2-OH-based perovskite film. Furthermore, the IPCE spectra of PHJ-PSCs based on PEDOT:PSS or PEDOT:PSS-NH_2-OH are measured, as shown in Fig. 6b, which displays the IPCE spectrum employed PEDOT:PSS-NH_2-OH shows a bit enhance than that with PEDOT:PSS at the whole wavelength range from 300 nm to 800 nm, it is helpful for improving the J_{sc}, and the integrated *Jsc* for PEDOT:PSS and PEDOT:PSS-NH_2-OH-based PHJ-PSCs is 19.4 mA/cm^2 and 18.9 mA/cm^2, respectively, which is in good agreement with the statistical J_{sc} in comparison with conventional photovoltaics (Table 1). On the other hand, the remarkable IPCE spectrum may partly suggests the efficient hole transport with good electron-blocking between perovskite and PEDOT:PSS-NH_2-OH layer. As a result, the increase in J_{sc} for PEDOT:PSS-NH_2-OH-based devices can be partly ascribed to the improved absorption.

The inner causes contributing to better property were investigated further. Steady PL presented a slightly efficient PL quench when depositing the $MAPbI_3$ atop of PEDOT:PSS-NH_2-OH HTL (Fig. 6c), indicating better hole extraction and transport capability from perovskite $MAPbI_3$ [28]. It is worth noting that there is a blue-shift of PL for PEDOT:PSS-NH_2-OH-based perovskite, of which dopamine semiquinone radical provides more electron donating effect for the trap passivation [10,11]. This result validates that faster and more efficient hole-extraction is achieved at the HTL/$MAPbI_3$ interface. Besides, time-resolved PL was measured as shown in Fig. 6d, based on the experimental results, we fitted the dated with the exponential fits ($y= y_0 + Ae^{-x/\tau}$), of which the lifetime is 31.8 ns and 17.6 ns for PEDOT:PSS and PEDOT:PSS-NH_2-OH-based perovskite film, respectively, which shows that the PL lifetime of the perovskite that deposited onto modified PEDOT:PSS layer decreased significantly, indicating efficient hole transfer occurred from perovskite to HTL [3].

In order to better understand the enhancement of photovoltaic parameters, especially for *FF* and V_{oc}, EIS was employed to explore the carrier transfer performance and recombination dynamics, as a consequence, series resistance (R_s), contact resistance (R_{sc}) and recombination resistance (R_{rec}) transport parameters can be obtained effectively, thereby physical processes of carrier transportation and recombination could be decoupled [13,29]. Fig. 7a–e present the Nyquist plot of PHJ-PSC devices with PEDOT:PSS and PEDOT:PSS-NH_2-OH HTL at DC bias of 0 V, 0.2 V, 0.4 V, 0.6 V and 0.8 V under one-sun AM1.5 illumination, respectively. The EIS pattern has the characteristics of arcs or transmission line. The equivalent circuit contain ideal capacitors and constant phase elements (CPE), as shown in Fig. 7f. It is obvious that the devices based on PEDOT:PSS-NH_2-OH have a low contact resistance R_{sc} than that of PEDOT:PSS. The R_{sc} is ascribed to selective contact layer/perovskite film, indicating that PEDOT:PSS-NH_2-OH is better than PEDOT:PSS for improving the charge extraction and transport [26]. Furthermore, it can been seen that the recombination resistance R_{rec} shows an obvious enhancement as

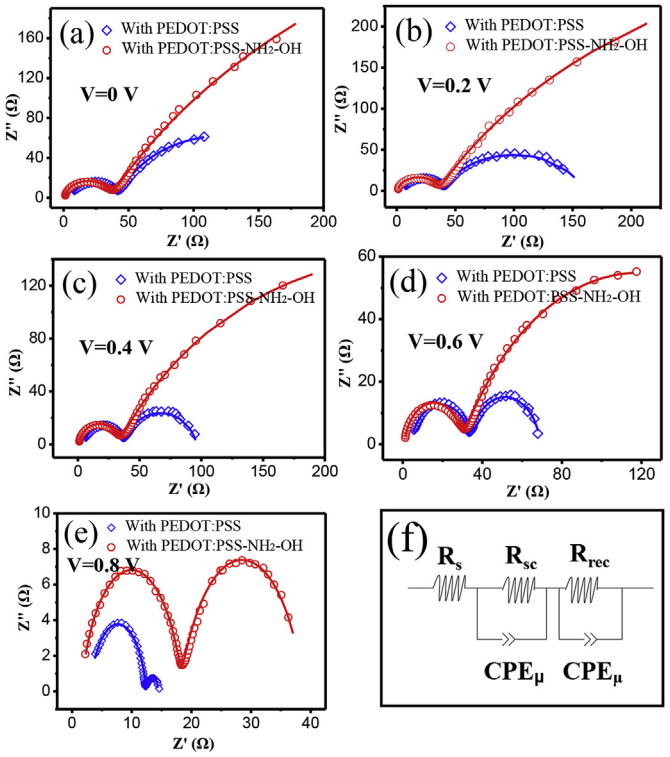

Fig. 7. (a–e) Nyquist plot of PHJ-PSC devices with PEDOT:PSS and PEDOT:PSS-NH_2-OH HTL at DC bias at 0–0.8 V with the interval of 0.2 V under one-sun AM1.5 illumination, respectively. (f) The equivalent circuit used for analysis in this work.

Table 2
Detailed numerical results of (a) R_s, (b) R_{sc} and (c) R_{rec} with PEDOT:PSS and PEDOT:PSS-NH_2-OH HTL that decoded from Nyquist plots.

Sample	DC Bias (V)	R_s (Ω)	R_{sc} (Ω)	R_{rec} (Ω)
With PEDOT:PSS	0	4.444	38.8	161.9
	0.2	4.559	36.02	118.9
	0.4	4.148	33.87	58.09
	0.6	4.162	29.75	35.48
	0.8	2.978	8.011	9.423
With PEDOT:PSS-NH_2-OH	0	1.094	34.35	937.7
	0.2	0.9198	34.14	898.9
	0.4	0.9495	31.83	473.2
	0.6	0.9081	28.61	179
	0.8	0.8569	16.65	20.6

employing PEDOT:PSS-NH_2-OH. The R_{rec} is mainly associated with the perovskite layer and its interface layer and is inversely proportion to recombination ratio [29], suggesting a lower recombination during the hole transport process as PEDOT:PSS-NH_2-OH was employed for HTL. As a consequence, it is reasonable to say that PEDOT:PSS-NH_2-OH is more favorable for carries transport than the traditional PEDOT:PSS material.

Specifically, the statistic R_s, R_{sc} and R_{rec} for the PHJ-PSC devices with PEDOT:PSS and PEDOT:PSS-NH_2-OH layers under AM 1.5 G with different bias voltages is presented in Figs. S2a–c and Table 2, which are deduced from the Nyquist plot. Generally speaking, the photovoltaic with low R_s and R_{sc} as well as large R_{rec} is beneficial for device performance owing to R_s is mainly associated with ITO and wire electrode, R_{sc} is ascribed to selective contacts or the interfaces adjacent to perovskite film, and R_{rec} is related to perovskite layer and its contact layers. A lower R_s or R_{sc} could be profitable for photon-generated carries transport at interface between perovskite and function layers (HTL or ETL), large R_{rec} could reduce the recombination ration of electrons and holes, making carries effectively migrate to electrodes [29]. Figs. S2a and b clearly show smaller resistance of R_s and R_{sc} for these devices that prepared by PEDOT:PSS-NH_2-OH HTL, along with the larger R_{rec} shown in Fig. S2c, implying a more favorable hole extraction and transport for photovoltaic devices [26].

4. Conclusions

In summary, stable semiquinone and amine radical modified PEDOT:PSS HTL material was used to fabricate PHJ-PSCs with a structure of ITO/PEDOT:PSS-NH_2-OH/$MAPbI_3$/PCBM/Al. As compared to the conventional photovoltaic device based on PEDOT:PSS, the PHJ-PSCs with PEDOT:PSS-NH_2-OH layer present an impressive preponderance, of which the best device with *PCE* up to 15.34% was achieved with negligible hysteresis regardless of different scanning directions and scanning speeds. Besides, the average *PCE* of twenty PHJ-PSC photovoltaic devices employed PEDOT:PSS-NH_2-OH HTL was increased from 10.67% to 14.16%, resulting in over 30% enhancement in *PCEs*. Meanwhile, all performance parameters distribution show more evenly with small standard deviations and demonstrated the good reproducibility and operability. The analysis of CV, PL, SEM and EIS indicated that the improvement of V_{oc}, J_{sc} and *FF* can be attributed to the four causes. 1) High radical content and strong charge extraction capability from perovskite to HTL. 2) Desirable energy level alignment with perovskite. 3) Favorable interaction with perovskite for high-quality film formation. 4) Efficient surface trap passivation effects for perovskite film. That is the HOMO level of PEDOT:PSS-NH_2-OH (−5.32 eV) matches well with the valence band of $MAPbI_3$ absorbers (−5.4 eV), and PHJ-PSCs have lower R_s and R_{sc}, higher R_{rec}, as well as outstanding incident photon-current conversion efficiency along with efficient hole transport and excellent electron blocking. The research work successfully demonstrated PEDOT:PSS-NH_2-OH is a good choice substitute for PEDOT:PSS as an excellent HTL material, showing great potential application for fabricating high-efficient PHJ-PSCs by low-temperature, solution process.

Acknowledgements

This work was supported by the National Natural Science Foundation of China (51673214, 21402054), the National Key Research and Development Program of China (2017YFA0206600), and the Hunan Provincial Natural Science Foundation of China (2015JJ1015). C.H.W. thanks the Master Innovation Fund of Central South University (2017ZZTS321). Y.L.G. acknowledges the support by National Science Foundation CBET-1437656. C.H.S and Y.L. thanks Pearl River S&T Nova Program of Guangzhou (201506010038, 201710010194).

Appendix A. Supplementary data

Supplementary data related to this article can be found at http://dx.doi.org/10.1016/j.jpowsour.2018.04.049.

References

[1] S.D. Stranks, G.E. Eperon, G. Grancini, C. Menelaou, M.J.P. Alcocer, T. Leijtens, L.M. Herz, A. Petrozza, H.J. Snaith, Science 342 (2013) 341–344.
[2] W. Yu, K.X. Wang, B. Guo, X.Q. Qiu, Y. Hao, J.J. Chang, Y. Li, J. Power Sources 358 (2017) 29–38.
[3] C.H. Wang, C.J. Zhang, S.T. Wang, G. Liu, H.Y. Xia, S.C. Tong, J. He, D.M. Niu, C.H. Zhou, K.X. Ding, Y.L. Gao, J.L. Yang, Sol. RRL 2 (2018) 1700209.
[4] Q.F. Xue, M.Y. Liu, Z.C. Li, L. Yan, Z.C. Hu, J.W. Zhou, W.Q. Li, X.F. Jiang, B.M. Xu, F. Huang, Y. Li, H.L. Yip, Y. Cao, Adv. Funct. Mater. (2018) 201707444.
[5] https://www.nrel.gov/pv/assets/images/efficiency-chart.png.
[6] H. Wu, C. Zhang, K. Ding, L. Wang, Y. Gao, J. Yang, Org. Electron. 45 (2017) 302–307.
[7] Y.D. Li, M.Y. Liu, Y. Li, K. Yuan, L.J. Xu, W. Yu, R.F. Chen, X.Q. Qiu, Hin-Lap Yip, Adv. Energy Mater. 7 (2017) 1601499.
[8] C. Zhang, Q. Luo, H. Wu, H. Li, J. Lai, G. Ji, L. Yan, X. Wang, D. Zhang, J. Lin,

L. Chen, J. Yang, C. Ma, Org. Electron. 45 (2017) 190–197.
[9] Q. Hu, H. Wu, J. Sun, D.H. Yan, Y.L. Gao, J.L. Yang, Nanoscale 8 (2016) 5350–5357.
[10] W.S. Liang, L.J. Xu, X.Q. Qiu, S. Sun, L.F. Lan, R.F. Chen, Y. Li, ACS Sustain. Chem. Eng. 5 (2016) 460–468.
[11] Y. Li, N.L. Hong, J. Mater. Chem. A 3 (2015) 21537–21544.
[12] P. Liu, X.L. Liu, L. Lyu, H.P. Xie, H. Zhang, D.M. Niu, H. Huang, C. Bi, Z.G. Xiao, J.S. Huang, Y.L. Gao, Appl. Phys. Lett. 106 (2015) 193903.
[13] C.H. Wang, J.L. Yang, Sci. China Mater 59 (2016) 743–756.
[14] J. Xiong, B.C. Yang, C.C. Cao, R.S. Wu, Y.L. Huang, J. Sun, J. Zhang, C.B. Liu, S.H. Tao, Y.L. Gao, J.L. Yang, Org. Electron. 30 (2016) 30–35.
[15] X.Y. Zhang, B. Zhang, X.H. Ouyang, L.H. Chen, H. Wu, J. Phys. Chem. C 121 (2017) 18378–18384.
[16] E. Zeglio, M.M. Schmidt, M. Thelakkat, R. Gabrielsson, N. Solin, O. Inganäs, Chem. Mater. 29 (2017) 4293–4300.
[17] F. Xie, W.C.H. Choy, C. Wang, S. Zhang, J. Hou, Adv. Mater. 25 (2013) 2051–2055.
[18] L. Cheng, Y. Hou, B. Zhang, S. Yang, J.W. Guo, L. Wua, H.G. Yang, Chem. Commun. 49 (2013) 5945–5947.
[19] K. Zilberberg, S. Trost, H. Schmidt, T. Riedl, Adv. Energy Mater 1 (2011) 377–381.
[20] J.A. Christians, R.C.M. Fung, P.V. Kamat, J. Am. Chem. Soc. 136 (2014) 758–764.
[21] J.Y. Jeng, K.C. Chen, T.Y. Chiang, P.Y. Lin, T.D. Tsai, Y.C. Chang, T.F. Guo, P. Chen, T.C. Wen, Y.J. Hsu, Adv. Mater. 26 (2014) 4107–4113.
[22] Z.L. Zhu, Y. Bai, T. Zhang, Z.K. Liu, X. Long, Z.H. Wei, Z.L. Wang, L.X. Zhang, J.N. Wang, F. Yan, S.H. Yang, Angew. Chem. Int. Ed. 53 (2014) 12571–12575.
[23] J.W. Jung, C.C. Chueh, A.K.Y. Jen, Adv. Mater. 27 (2015) 7874–7880.
[24] L. Hu, W.W. Wang, H. Liu, J. Peng, H.F. Cao, G. Shao, Z. Xia, W.L. Ma, J. Tang, J. Mater. Chem. A 3 (2015) 515–518.
[25] K. Zhao, R. Munir, B. Yan, Y. Yang, T. Kim, A. Amassian, J. Mater. Chem. A 3 (2015) 20554–20559.
[26] J. Huang, K.X. Wang, J.J. Chang, Y.Y. Jiang, Q.S. Xiao, Y. Li, J. Mater. Chem. A 5 (2017) 13817–13822.
[27] J. Xiong, B. Yang, R. Wu, C. Cao, Y. Huang, C. Liu, Z. Hu, H. Huang, Y. Gao, J. Yang, Org. Electron. 24 (2015) 106–112.
[28] C.H. Wang, C.J. Zhang, S.T. Tong, J.Q. Shen, C. Wang, Y.Z. Li, S. Xiao, J. He, J. Zhang, Y.L. Gao, J.L. Yang, J. Phys. Chem. C 121 (2017) 6575–6580.
[29] R.S. Wu, J.L. Yang, J. Xiong, P. Liu, C.H. Zhou, H. Huang, Y.L. Gao, B.C. Yang, Org. Electron. 26 (2015) 265–272.
[30] J. Qiu, Y. Qiu, K. Yan, M. Zhong, C. Mu, H. Yan, S. Yang, Nanoscale 5 (2013) 3245–3252.
[31] J.H. Im, C.R. Lee, J.W. Lee, S.W. Park, N.G. Park, Nanoscale 3 (2011) 4088–4093.
[32] W. Y Nie, H. Tsai, R. Asadpour, J. Blancon, A.J. Neukirch, G. Gupta, J.J. Crochet, M. Chhowalla, S. Tretiak, M.A. Alam, H. Wang, A.D. Mohite, Science 347 (2015) 522–525.